The Astrophysical Journal, 970:6 (12pp), 2024 July 20 https://doi.org/10.3847/1538-4357/ad4ee1

The Peculiar Precursor of a Gamma-Ray Burst from a Binary Merger Involving a Magnetar

Shuo Xiao[1,2,3], Yan-Qiu Zhang[2,3], Zi-Pei Zhu[4,5], Shao-Lin Xiong[2], He Gao[6], Dong Xu[4], Shuang-Nan Zhang[2], Wen-Xi Peng[2], Xiao-Bo Li[2], Peng Zhang[7], Fang-Jun Lu[2], Lin Lin[6], Liang-Duan Liu[8], Zhen Zhang[2], Ming-Yu Ge[2], You-Li Tuo[2], Wang-Chen Xue[2,3], Shao-Yu Fu[4], Xing Liu[4,9], Jin-Zhong Liu[10,11], An Li[6], Tian-Cong Wang[6], Chao Zheng[2,3], Yue Wang[2], Shuai-Qing Jiang[4], Jin-Da Li[6], Jia-Cong Liu[2,3], Zhou-Jian Cao[6], Xi-hong Luo[1], Jiao-jiao Yang[1], Shu-Xu Yi[2], Xi-Lu Wang[2], Ce Cai[2,3,12], Qi-Bin Yi[2,13], Yi Zhao[2,6], Sheng-Lun Xie[2,8], Cheng-Kui Li[2], Qi Luo[2,3], Li-Ming Song[2], Shu Zhang[2], Jin-Lu Qu[2], Cong-Zhan Liu[2], Xu-Fang Li[2], Yu-Peng Xu[2], and Ti-Pei Li[2,3,14]
[1] School of Physics and Electronic Science, Guizhou Normal University, Guiyang 550001, People's Republic of China
[2] Key Laboratory of Particle Astrophysics, Institute of High Energy Physics, Chinese Academy of Sciences, 19B Yuquan Road, Beijing 100049, People's Republic of China; xiongsl@ihep.ac.cn, gaohe@bnu.edu.cn
[3] University of Chinese Academy of Sciences, Chinese Academy of Sciences, Beijing 100049, People's Republic of China
[4] Key Laboratory of Space Astronomy and Technology, National Astronomical Observatories, Chinese Academy of Sciences, Beijing 100012, People's Republic of China; dxu@nao.cas.cn
[5] Department of Astronomy, School of Physics, Huazhong University of Science and Technology, Wuhan 430074, People's Republic of China
[6] Department of Astronomy, Beijing Normal University, Beijing 100875, People's Republic of China; zhangsn@ihep.ac.cn
[7] College of Science, China Three Gorges University, Yichang 443002, People's Republic of China
[8] Department of Physics, Central China Normal University, Wuhan 430079, People's Republic of China
[9] Key Laboratory of Cosmic Rays, Ministry of Education, Tibet University, Lhasa, Tibet 850000, People's Republic of China
[10] Xinjiang Astronomical Observatory, Chinese Academy of Sciences, Urumqi, Xinjiang 830011, People's Republic of China
[11] School of Astronomy and Space Science, University of Chinese Academy of Sciences, Beijing 100049, People's Republic of China
[12] College of Physics, Hebei Normal University, 20 South Erhuan Road, Shijiazhuang 050024, People's Republic of China
[13] School of Physics and Optoelectronics, Xiangtan University, Yuhu District, Xiangtan, Hunan 411105, People's Republic of China
[14] Department of Astronomy, Tsinghua University, Beijing 100084, People's Republic of China
Received 2024 March 11; revised 2024 April 21; accepted 2024 May 9; published 2024 July 11

Abstract

The milestone discovery of GW170817-GRB 170817A-AT 2017gfo has shown that gravitational waves (GWs) could be produced during the merger of a neutron star–neutron star/black hole and that in electromagnetic (EM) waves, a gamma-ray burst (GRB) and a kilonova (KN) are generated in sequence after the merger. Observationally, however, EM properties before the merger phase are still unclear. Here we report a peculiar precursor in a KN-associated long-duration GRB 211211A, providing evidence of the EM before the merger. This precursor lasts ∼0.2 s, and the waiting time between the precursor and the main burst is ∼1 s, comparable to that between GW170817 and GRB 170817A. The spectrum of the precursor could be well fit with a nonthermal cutoff power-law model instead of a blackbody. In particular, a ∼22 Hz quasiperiodic oscillation candidate ($\sim 3\sigma$) is detected in the precursor. These temporal and spectral properties indicate that this precursor is probably produced by a catastrophic flare accompanied with magnetoelastic or crustal oscillations of a magnetar in a binary compact merger. The strong magnetic field of the magnetar can also account for the prolonged duration of GRB 211211A. However, it poses a challenge to reconcile the rather short lifetime of a magnetar with the rather long spiraling time of a binary neutron star system only by the GW radiation before the merger.

Unified Astronomy Thesaurus concepts: Gamma-ray bursts (629)

1. Introduction

As the most violent explosions in the Universe (Zhang 2018), gamma-ray bursts (GRBs) are traditionally classified into long GRBs (LGRBs) and short GRBs (SGRBs) based on their durations separated at ∼2 s (Kouveliotou et al. 1993). Some characteristics and empirical relationships, such as hardness ratio, spectral lag, minimum variability timescale, and Amati relation (Amati et al. 2002; Zhang et al. 2009) are also employed to determine whether a GRB originates from massive star core collapse, or from binary neutron star mergers (Woosley & Bloom 2006; Abbott et al. 2017) where a kilonova may be observed owing to *r*-process nucleosynthesis (Li & Paczyński 1998; Wu et al. 2017).

About 10% of GRBs (mostly LGRBs) detected by Swift/BAT have precursors, and no significant difference was found between the precursor and the main emission, implying that the precursor shares the same physical origin with the main burst and directly originates from central engine activities (Hu et al. 2014; Li & Mao 2022). On the other hand, SGRBs with precursors are very rare. Only about 2.7% of SGRBs detected by Swift/Burst Alert Telescope (BAT) and Fermi/Gamma-ray Burst Monitor (GBM) have precursors. As of 2020 April, Fermi/GBM only detected about 16 precursors in SGRBs (Wang et al. 2020).

The thermal-spectrum precursor of an SGRB is usually attributed to shock breakout or photospheric radiation of a fireball launched after the merger, whereas the nonthermal precursor is mostly interpreted with magnetospheric interaction between two neutron stars (Hansen & Lyutikov 2001;

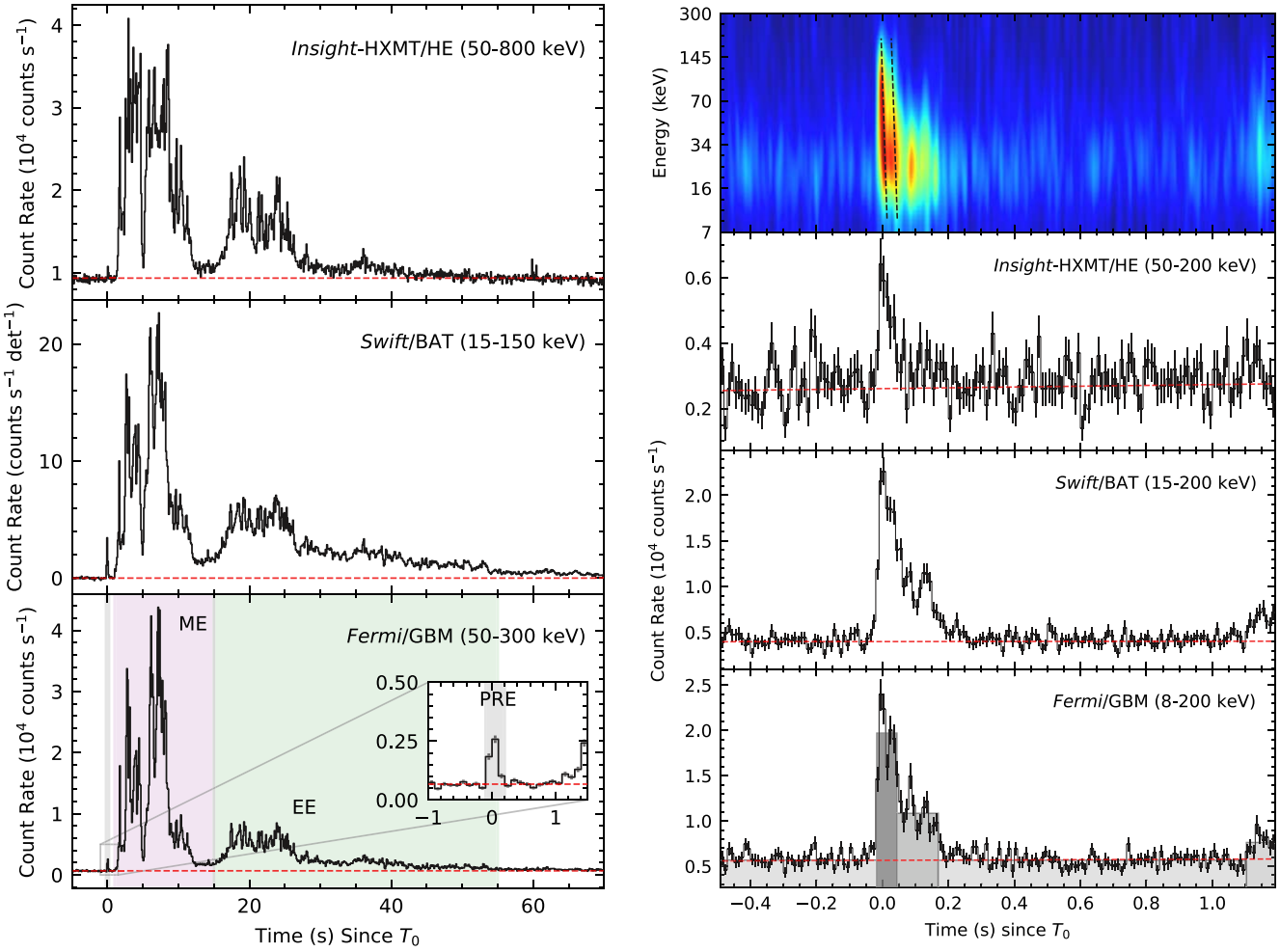

Figure 1. Left panels: lightcurves of GRB 211211A. The top panel is the summed Insight-HXMT/HE lightcurve in the 50–800 keV energy range (the incident energy greater than ∼100 keV). The second panel is the summed Swift/BAT mask-weighted and background-subtracted lightcurve in the 15–150 keV energy range. The third panel is the summed Fermi/GBM lightcurve in the 50–300 energy range. Right panels: lightcurves of the precursor observed by Insight-HXMT/HE, Swift/BAT, and Fermi/GBM, the time bin is 10 ms. The light travel time difference has been corrected. The $T_{\rm pre}$ and $T_{\rm wt}$ at 8–200 keV band are about 0.19 s and 0.93 s, respectively. The shaded bars in the bottom panel show the lightcurve structure obtained by the BB algorithm. The black dashed lines in the top panel represent logarithmic spectral lag behavior on a time-energy domain, $t(E) = 0.006\ln(E) + C$.

Troja et al. 2010; Palenzuela et al. 2013; Wang et al. 2018) or the crust resonant shattering of a neutron star (Tsang et al. 2012) prior to the merger. As shown in the spectral analysis of SGRB precursors observed by Fermi/GBM (Wang et al. 2020), there is no "decisive" evidence of a nonthermal spectrum (ΔBIC < 6) for any precursor yet. In another study with Swift and Fermi/GBM data (Zhong et al. 2019), some candidate precursors prefer a nonthermal cutoff power-law (CPL) model with ΔBIC > 10, but none of these events satisfies the precursor criteria strictly. Indeed, it is very difficult to constrain the energy spectrum of SGRB precursors because they are usually very weak with limited statistics.

In this work, observations of GRB 211211A are briefly described in Section 2, and the identification, and temporal and spectral analyses of the precursor are presented in Section 3. Finally, the discussion and conclusion are given in Sections 4 and 5, respectively.

2. Observations

GRB 211211A was detected at 2021-12-11 13:09:59.651 (UTC, denoted as T_0) by Fermi/GBM (Mangan et al. 2021), Swift/BAT (D'Ai et al. 2021), and Insight-HXMT/HE (Zhang et al. 2021). The full burst lightcurve can be divided into three emission episodes: a precursor (PRE) with a duration of ∼0.2 s in fast-rising exponential decay (FRED) shape (as shown in Figure 1), a ∼10 s spiky hard main emission (ME), and a soft long extended emission (EE) with >50 s (Mangan et al. 2021). This burst has a duration of $T_{90} \sim 34.3$ s in 10–1000 keV by Fermi/GBM (Mangan et al. 2021).

With detailed analysis of the prompt emission, we find that the spectral and temporal properties, which include a small minimum variability timescale (8.5 ± 0.8 ms) calculated by the Bayesian Blocks (BB) algorithm (Scargle et al. 2013; Xiao et al. 2023), small spectral lag (3.6 ± 1.6 ms between 200–250 keV and 100–150 keV) calculated by the Li-cross-correlation function (CCF) method (Li et al. 2004; Xiao et al. 2022a), as well as the positions in $T_{90} - E_{\rm peak}$ and Amati correlation diagrams (Mei et al. 2022; Troja et al. 2022; Yang et al. 2022; Gompertz et al. 2023), confirm that GRB 211211A originates from a compact binary merger.

On the other hand, no accompanied supernovae but an AT 2017gfo-like kilonova was reported for this burst (Rastinejad et al. 2022), which was also confirmed by the Nanshan/NEXT 0.6 m telescope. Optical follow-ups at the Nanshan/NEXT

Table 1
Identification of the Precursor of GRB 211211A

Instrument	T_{pre} (s)	T_{wt} (s)	b_0[a] (counts s^{-1})	b_1[a] (counts s^{-2})	χ^2/dof	p-value	A^2/n	Significance
Insight-HXMT/HE	0.08 (0.00:0.08)	1.28 (0.08:1.35)	2610.40 ± 135.23	61.45 ± 101.37	74.69/86	0.80	0.30/88	$>15\sigma$
Swift/BAT	0.22 (0.00:0.22)	0.88 (0.22:1.10)	3985.38 ± 165.82	17.21 ± 135.69	73.48/86	0.83	0.27/88	$>15\sigma$
Fermi/GBM	0.19 (−0.01:0.17)	0.93 (0.17:1.10)	5651.43 ± 174.77	62.74 ± 136.93	90.18/86	0.36	0.31/88	$>15\sigma$

Note.
[a] b_0 is the background rate at T_0, and b_1 is the background change rate.

0.6 m telescope localized the burst in a bright ($r = 19.5$) galaxy SDSS J140910.47+275320.8, for which a spectroscopic redshift of $z = 0.076$ was reported by the Nordic Optical Telescope (Malesani et al. 2021). The offset between the burst and the nucleus of the galaxy of $5\farcs11 \pm 0\farcs23$, corresponding to 7.61 ± 0.34 kpc in projection, indicates a very small probability of chance coincidence of 1.1% (Bloom et al. 2002). Considering the measured distance, the isotropic equivalent energies E_{iso} for PRE, ME, and EE of GRB 211211A are 6.97×10^{48} erg, 9.02×10^{51} erg, and 2.60×10^{51} erg, respectively.

3. The Peculiar Precursor

3.1. Identification of Precursor

A precursor should satisfy the following requirements (Wang et al. 2020): (1) it should be the first pulse in the lightcurve; (2) the peak count rate is lower than that of the main pulse; (3) the count rate during the waiting time period, i.e., the time interval between the precursor and the main pulse, is consistent with the background level; (4) it is significant enough to be identified as a burst signal.

The BB algorithm (Scargle et al. 2013) is widely used to identify the precursor (Hu et al. 2014; Wang et al. 2020) of GRBs. Here we employ the same technique to confirm the existence of the precursor of GRB 211211A. Table 1 lists the results of the precursor and waiting time obtained from the BB algorithm.

For the third criterion, two statistical schemes are adopted to test whether the lightcurve during the waiting time period is consistent with the background. We first calculate the significance of the "possible weak signal" within T_{wt} by the Li–Ma formula (Li & Ma 1983). After choosing the quiescent period determined by the BB algorithm as t_{on} and the confirmed background region from $T_0 - 1.1$ s to $T_0 - 0.1$ s as t_{off}, the Li–Ma formula gives a significance of 0.5σ for GBM and 1.7σ for BAT, which are consistent with background fluctuation.

To further investigate the lightcurve behavior during the waiting time period, we fit the $T_0 - 1.1$ s to $T_0 - 0.1$ s background lightcurves of three instruments with a first-order polynomial and interpolate over $T_0 - 0.5$ s to $T_0 + 1.25$ s, then the estimate of the background rate is obtained. The significance of a potential signal relative to the background noise level can be calculated by weighting the difference between the lightcurve and estimated background, this quantity is commonly referred to as χ. We apply the χ^2 and Anderson–Darling test to examine the overall fluctuation and normality of χ within this period, respectively. As shown in Figure 1, the large p-value of the χ^2 test implies the overall fluctuation of χ is consistent with the background, and the high significance of the Anderson–Darling test shows the good normality of χ, i.e., the lightcurves behave like the background. All the statistical evidence indicates that there exists no significant signal in the quiescent period, thus the signal near T_0 should be identified as the precursor of the GRB. The precursor is well separated from the main burst by a quiescence period (T_{wt}) of about 1 s, during which the lightcurve decreases to the background. We note that this is the only quiescence time interval found throughout the entire burst.

Interestingly, we find that none of the GRBs with confirmed or candidate kilonova reported earlier (Jin et al. 2020), including GRB 050709, GRB 060614, GRB 061201, GRB 070809, GRB 130603B, GRB 150101B, GRB 160621B, and GRB 170817A, have a precursor (Zhong et al. 2019; Wang et al. 2020). Recently, GRB 200522A has been reported to have a precursor but the kilonova is not confirmed (O'Connor et al. 2021). GRB 230307A has a confirmed kilonova (Gillanders et al. 2023; Levan et al. 2024; Yang et al. 2024) but the suggested precursor candidate (Dichiara et al. 2023) does not strictly meet the criteria of quiescence period between the precursor and main burst. Therefore, the precursor of GRB 211211A seems to be the only one in the GRBs with confirmed kilonova so far.

3.2. Temporal and Spectrum Analysis

The overall shape of the precursor lightcurve can be fitted well with the FRED model, with the rising time of $8.0^{+2.4}_{-2.2}$ ms, $10.0^{+2.1}_{-2.2}$ ms, and $10.4^{+12.2}_{-6.4}$ ms and the decay time of $84.0^{+10.8}_{-10.7}$ ms, $99.2^{+8.0}_{-8.4}$ ms, and $43.1^{+12.0}_{-12.3}$ ms for Fermi/GBM, Swift/BAT, and HXMT/HE data, respectively. With the BB algorithm, we calculate the duration of the precursor as $T_{pre} \sim 0.19$ s (T_0-0.017 to T_0+0.17 s) for GBM (8–200 keV), ∼0.2 s for BAT (15–200 keV), and ∼0.1 s for HXMT/HE (50–200 keV), and the waiting time between the precursor and the main burst as $T_{wt} \sim 0.93$ s (T_0+0.17 to T_0+1.10 s) for GBM, ∼0.88 s (BAT), and ∼1.28 s (HXMT/HE). Interestingly, this precursor follows well the relation between the waiting time and precursor duration of SGRBs (see Figure 2), lending additional support to the merger origin despite the prolonged main burst. However, this precursor is the outlier in T_{grb}–T_{wt} and T_{grb}–T_{pre} relationships (see Figure 2) owing to the prolonged main burst.

Spectrum fitting for the precursor has been performed with Fermi/GBM and Insight-HXMT data. The Bayesian information criterion (BIC; Schwarz 1978) is used to measure the goodness of fit and determine the best model. CPL, blackbody, and CPL + blackbody models are used (see Table 2). Since the CPL-only model compared to the CPL + blackbody model yields $\Delta BIC > 8$, and the CPL model compared to the blackbody model (Figure (3)) yields $\Delta BIC > 155$, we find that the best model of the precursors is the nonthermal spectrum (CPL), which displays "decisive" evidence (Liddle 2007) against the models with higher criterion values.

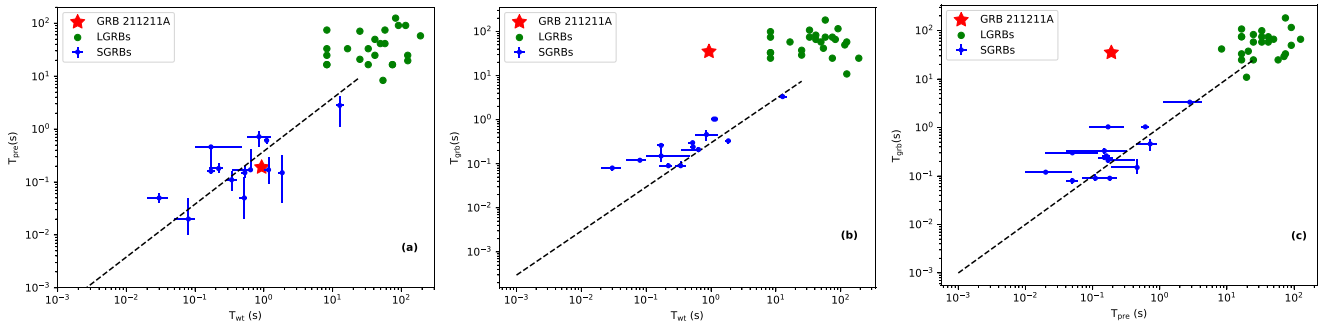

Figure 2. (a) The waiting time T_{wt} vs. the full duration of the precursor emission T_{pre}. (b) T_{wt} vs. the full duration of the GRB T_{grb}. (c) T_{pre} vs. T_{grb}. The GRB sample is obtained from the literature (Hu et al. 2014; Wang et al. 2020).

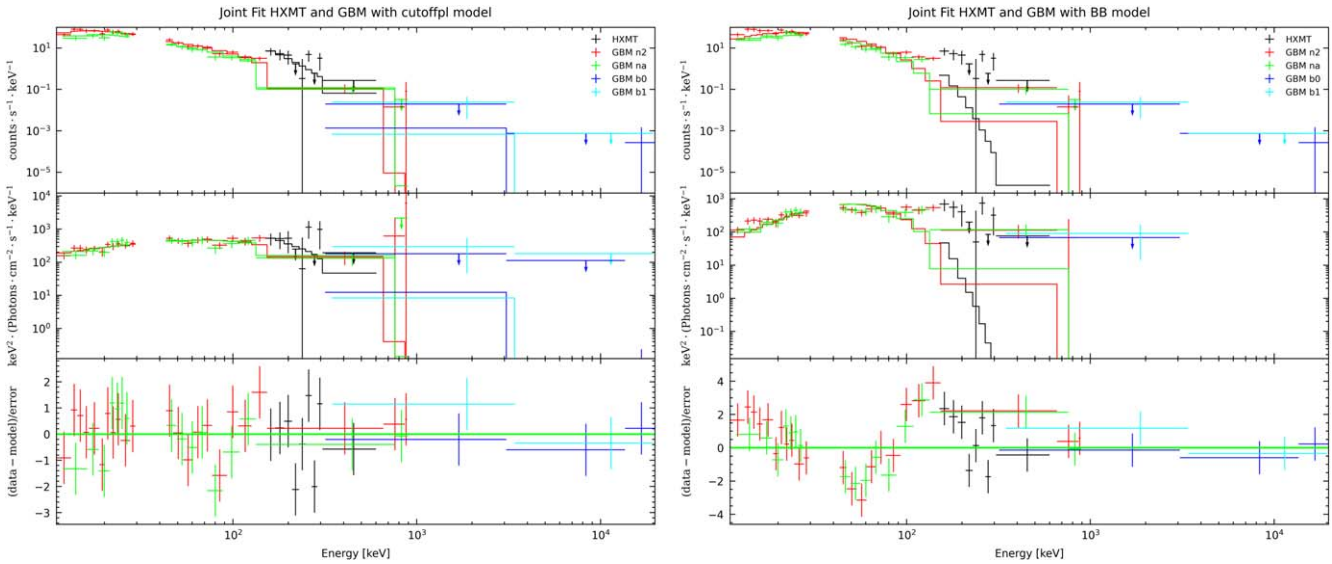

Figure 3. The spectral fitting with the CPL model (left panel) and blackbody model (right panel) of the precursor with Fermi/GBM and Insight-HXMT/HE for GRB 211211A.

Table 2
The Spectral Fitting with Different Models of the Precursor with Fermi/GBM and Insight-HXMT/HE for GRB 211211A

Model	α	E_{cut} (keV)	KT (keV)	Flux (erg cm^{-2} s^{-1})	pgstat/dof	BIC
CPL	$-1.03^{+0.15}_{-0.15}$	...	$70.74^{+17.71}_{-10.81}$	$1.76^{+0.08}_{-1.04} \times 10^{-6}$	376/200	397.36
CPL+blackbody	$-0.81^{+0.30}_{-0.10}$	$71.88^{+19.16}_{-9.38}$	$7.73^{+2.72}_{-1.37}$	$1.80^{+0.03}_{-1.18} \times 10^{-6}$	373/198	404.95
Blackbody	...	...	$13.32^{+0.60}_{-0.49}$	$1.51^{+0.11}_{-0.11} \times 10^{-6}$	536/201	551.84

The energy spectra of all SGRB precursors observed by the GBM have been stringently searched and studied in the literature (Wang et al. 2020), but none of them has "decisive" evidence of a nonthermal spectrum (ΔBIC < 6). On the other hand, the precursors of SGRBs observed by Swift and GBM are investigated in the literature (Zhong et al. 2019), and although several of them prefer CPL with ΔBIC > 10, none of these strictly satisfies the precursor criteria, i.e., the count rate during the waiting time period is consistent with the background level (e.g., GRB 160726A) or a significance high enough to be identified as signal (e.g., GRB 180402A and bn 160818198), or it should be an LGRB (e.g., GRB 140209A). Therefore, the precursor of GRB 211211A is a rare burst confirmed with a nonthermal spectrum in the SGRB precursors (merger origin) thanks to its high brightness.

For this precursor, the average flux is $1.76^{+0.08}_{-1.04} \times 10^{-6}$ erg cm^{-2} s^{-1}, the time-averaged isotropic luminosity is $2.53^{+0.06}_{-0.47} \times 10^{49}$ erg s^{-1}, the 64 ms peak isotropic luminosity is $7.66^{+0.36}_{-1.19} \times 10^{49}$ erg s^{-1} and the total isotropic energy is $6.97^{+0.15}_{-1.29} \times 10^{48}$ erg, considering the distance of 346.1 Mpc, which is derived from the redshift measurement.

In addition, we find that spectral analysis jointly with Fermi/GBM and HXMT/HE data show significant spectral evolution in PRE, ME, and EE episodes (Table 3). As shown in Figure 3, the spectrum of the precursor is significantly softer than ME. The spectral lags (100–300 keV compared to 8–50 keV) in different time ranges observed by Fermi/GBM are shown in Figure 4. The spectral lag of the precursor is slightly larger than that of the main pulses during the ME, which is confirmed by an independent study (Troja et al. 2022). We further investigate

Table 3
Spectral Fitting with Fermi/GBM and Insight-HXMT/HE for GRB 211211A

Episode	Model	$E^{*}_{\rm cut,1}$ (keV)	α_1	β	$E_{\rm cut,2}$[a] (keV)	α_2	$E_{\rm iso}$ (erg)	E_γ[b] (erg)	pgstat/dof
Precursor	CPL	⋯	⋯	⋯	71 ± 15	-1.03 ± 0.16	$6.97^{+0.15}_{-1.29} \times 10^{48}$	⋯	376/200
Main emission	Band+CPL	97 ± 14	-0.41 ± 0.14	-2.04 ± 0.02	1377 ± 56	-1.01 ± 0.04	$9.02^{+0.02}_{-0.17} \times 10^{51}$	4.06×10^{48}	852/438
Extended emission	Band+CPL	32 ± 8	-0.38 ± 0.33	-2.16 ± 0.04	434 ± 82	-1.25 ± 0.16	$2.60^{+0.11}_{-1.49} \times 10^{51}$	1.26×10^{48}	840/807
Full burst	Band+CPL	63 ± 10	-0.56 ± 0.14	-1.96 ± 0.02	1229 ± 81	-1.18 ± 0.05	$1.15^{+0.01}_{-0.03} \times 10^{52}$	⋯	1096/388

Notes.
[a] $E_{\rm cut} = E_{\rm peak}/(2+\alpha)$. The subscripts 1 and 2 in $E^{*}_{\rm cut,1}$ and $E_{\rm cut,2}$ represent the parameters of Band and CPL, respectively.
[b] Corrected for beaming effect with a jet half-opening angle of 0.05 rad.
[c] HXMT data are only used for spectral fitting in the precursor and extended emission.

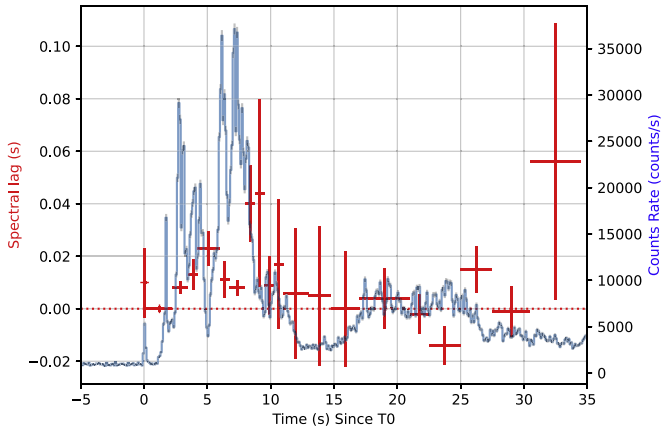

Figure 4. Spectral lag (100–300 keV compared to 8–50 keV) evolution in GRB 211211A. The detector n2 with the optimal incidence angle is used.

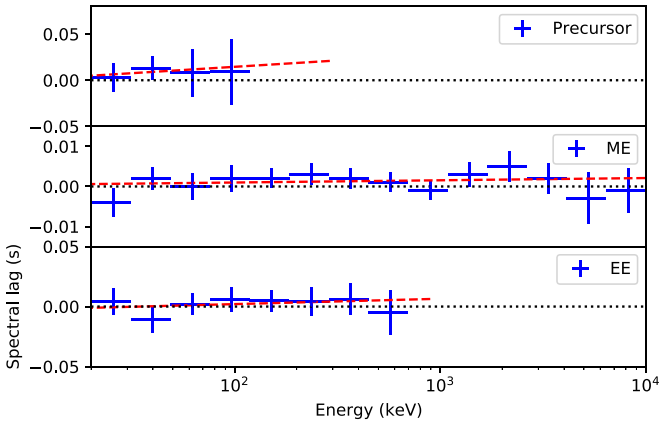

Figure 5. Energy-dependent spectral lag between the lowest energy band (8–12 keV) and any higher energy band. The detectors n2 and b0 with the optimal incidence angles are used. From top to bottom panels are the spectral lags of Precursor, ME, and EE, which can be fitted with $t(E) \approx 0.006(\pm0.002)\ln(E) - 0.013$ s, $t(E) \approx 0.0002(\pm0.0003)\ln(E) - 0.0001$ s, and $t(E) \approx 0.002(\pm0.002)\ln(E) - 0.007$ s, respectively.

the relationship between spectral lags and energy bands and obtain similar results, as shown in Figure 5. Besides, we find the minimum variability timescale of the precursor is 15 ± 2 ms, which is slightly larger compared to that of the main emission (8.5 ± 0.8 ms). These temporal and spectral characteristics also indicate that the origin of this precursor should be different from the main burst.

3.3. Quasiperiodic Oscillation Candidate

More interestingly, we find that there are several regularly spaced pulses superimposed on the FRED trend in the precursor lightcurves (from $T_0-0.1$ s to $T_0+0.3$ s) of Fermi/GBM and Swift/BAT, which inspired us to search for quasiperiodic oscillation (QPO; see Figure 6). We estimate the significance of QPO using Gaussian processes (GP), Z^2, fast Fourier transform, weighted wavelet Z-transform (WWZ), and the Lomb–Scargle Periodogram (LSP) methods, respectively. Note that we do not consider the trial numbers of QPO search in other SGRBs with precursors in the estimation of QPO significance, because this GRB 211211A is unique as a long-duration kilonova-associated merger-origin SGRB.

3.3.1. Gaussian Processes Method

Time-series data can be used to investigate QPO directly in the time domain using GP regression (Hübner et al. 2022b). We model QPOs as a stochastic process on top of a deterministic shape and perform model selection between QPOs and red noise (see Hübner et al. 2022b for details). We obtain that $\ln BF_{\rm qpo}$ for GBM data is 2.5. The Bayes factor $BF_{\rm qpo}$ is defined as

$$BF_{\rm qpo} = \frac{Z(d|k_{\rm qpo+rn}, \mu)}{Z(d|k_{\rm rn}, \mu)}, \quad (1)$$

where the numerator (i.e., QPO and red noise) and denominator (i.e., red noise) are the respective evidence in the different models.

We perform this analysis for 1000 simulated lightcurves produced for each set of parameters and find that the p-value is 0.006, corresponding to 2.5σ. In this work, we adopt the publicly available code of GP released by Hübner et al. (2022b).

3.3.2. The Z^2 Method

We also use the GBM data to search for periodic signals with Z^2 (the harmonic = 1) around 25 Hz in the precursor via *stingray* (Bachetti et al. 2022) and find QPOs of ∼23.49 Hz with a significance of about 6.6σ. The same analyses were applied to the BAT data that revealed QPOs at 21.87 Hz with a significance of 4.0σ. It is worth noting that the number of trials of frequencies searched is considered throughout this work. The QPO significance is 8.3σ by combining the data of GBM and BAT. However, we note here that the significance of the Z^2 method may be overestimated (Hübner et al. 2022a)

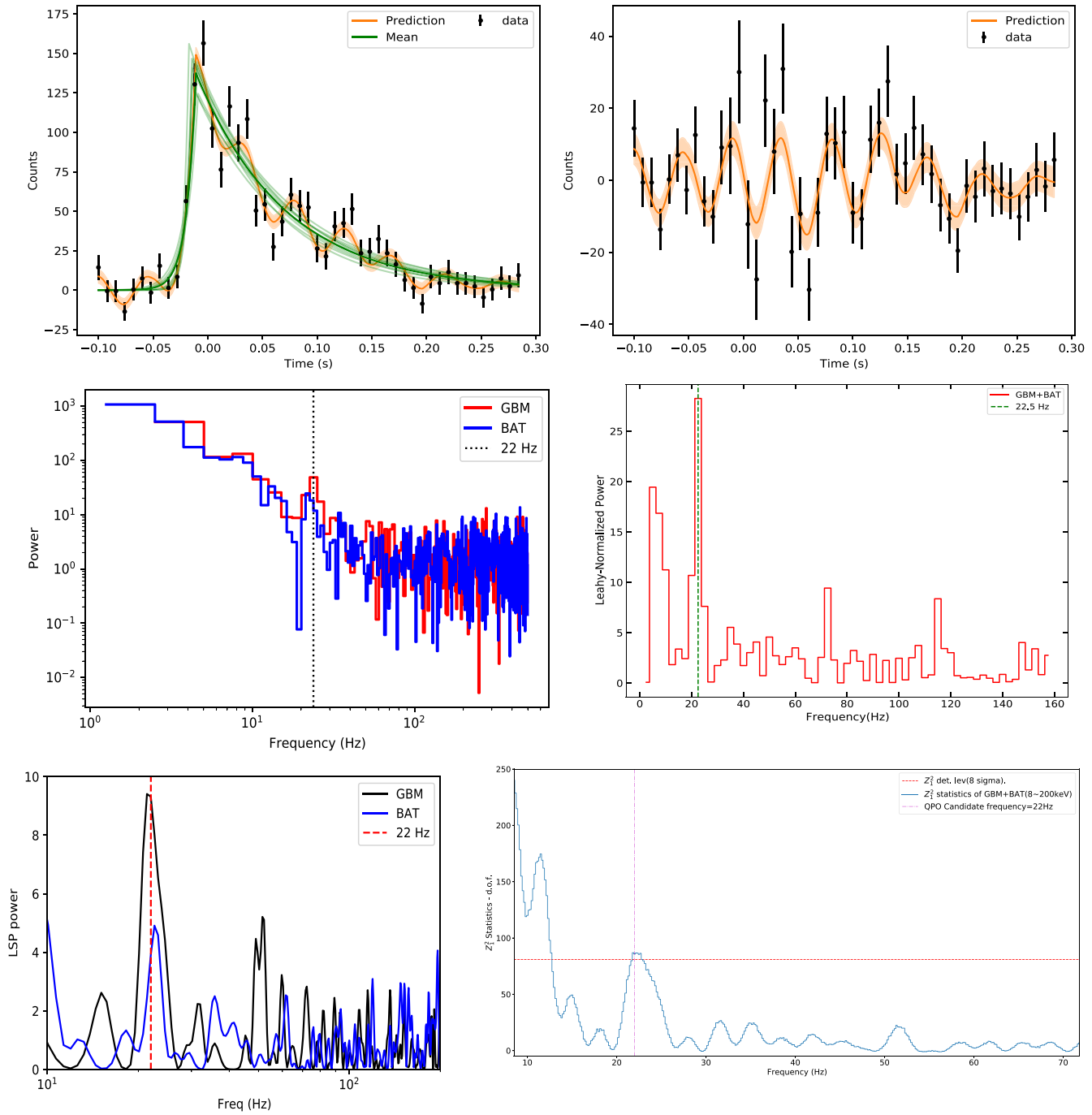

Figure 6. Top panels: the lightcurve of GBM and the maximum likelihood fit (top left), and the residual lightcurve minus and the maximum likelihood prediction (top right), the time bin is 8 ms. The significance level is 2.5σ. Middle panels: the Leahy normalized power of Fermi/GBM and Swift/BAT with the lightcurves (middle left) and FRED-model-subtracted lightcurves (middle right). The QPO significance is 3.8σ by combining the lightcurves of GBM and BAT. Bottom left panel: LSP power of GRB 211211A in 8–200 keV at −0.1 s to 0.3 s. The black and blue solid lines represent LSP power of GBM and BAT, respectively. The red dashed line (22 Hz) represents QPO frequency obtained from WWZ. Bottom right panel: Z_1^2 Periodograms for GBM and BAT observations using event-by-event data, the QPO significance is 8.3σ by combining the data of GBM and BAT. The trials of frequencies searched are considered here.

due to the deviation from the standard χ^2 − distribution at each frequency.

3.3.3. The Fast Fourier Transform Method

We perform Fast Fourier analysis on the GBM and BAT lightcurves with FRED subtracted, respectively. In order to estimate the significance of the 22.5 Hz QPOs, we use Monte Carlo simulations, a widely used tool to evaluate the timing results on a transient event whose profile is known. Specifically, for this precursor, we adopt the FRED function to fit the GBM and BAT lightcurves and then utilize the Markov Chain Monte Carlo simulations to generate many sets of FRED parameters of posterior probabilities. With each set of parameters, a FRED profile between −0.1 s and 0.3 s can be generated and a simulated lightcurve can be produced by adding the Poisson photon counting noise. Each simulated lightcurve will give a periodogram, and thus one can get the distribution of the periodograms at different Fourier frequencies.

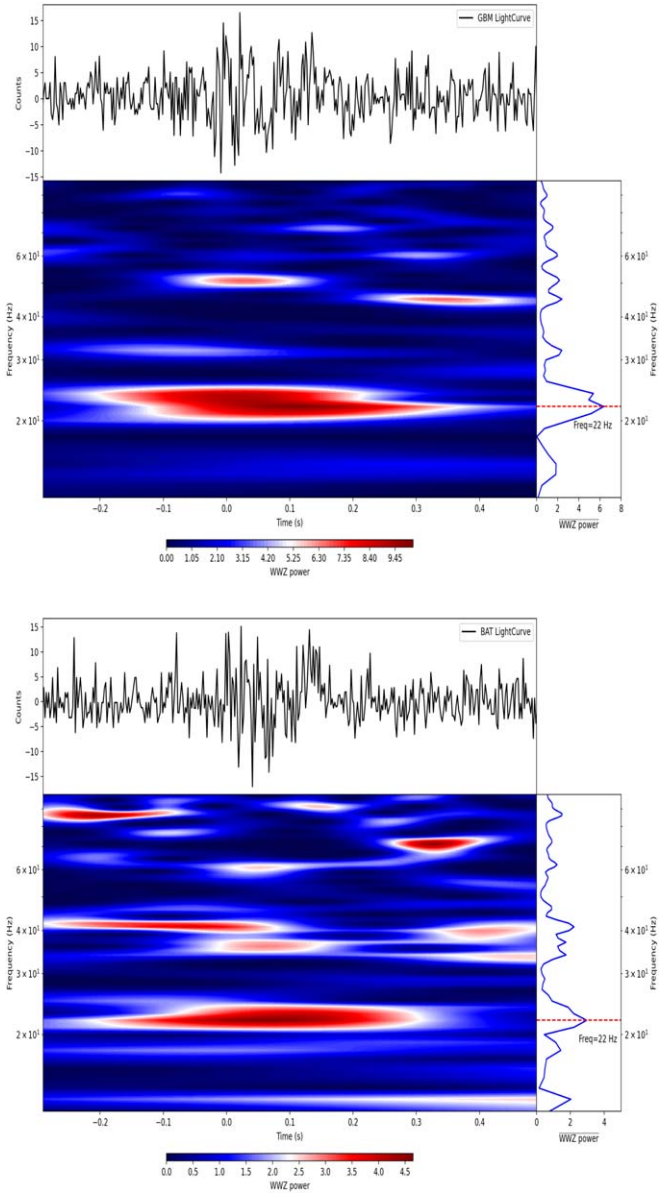

Figure 7. FRED-subtracted precursor lightcurve of GBM (upper panel) and BAT (lower panel) in 8–200 keV and the 2D-contour plots of WWZ power. The blue solid lines represent the time-averaged WWZ power, respectively. The significance levels for GBM and BAT are 3.0σ and 2.0σ, respectively.

The probability value of the QPOs can be obtained by comparing the Leahy power (Van der Klis 1989) at 22.5 Hz of the observed lightcurve to those from the above simulations, which is 0.0016 for GBM and 0.086 for BAT, corresponding to 2.9σ and 1.3σ, respectively. The QPO significance is 3.8σ by combining the lightcurves of GBM and BAT. The number of trials of frequencies searched is considered here.

3.3.4. The Weighted Wavelet Z-transform Method and the Lomb–Scargle Periodogram Method

We first employ one of the most widely used methods, the WWZ (Foster 1996), to obtain the power spectra of GBM and BAT lightcurves with FRED subtracted. Strong peaks at 22^{+3}_{-2} Hz (GBM) and 22^{+3}_{-1} Hz (BAT) (with the period cycle of 45^{+5}_{-4} ms (GBM) and 45^{+5}_{-2} ms (BAT); Figure (7)) are found in the WWZ power spectra, suggesting the existence of QPOs. The

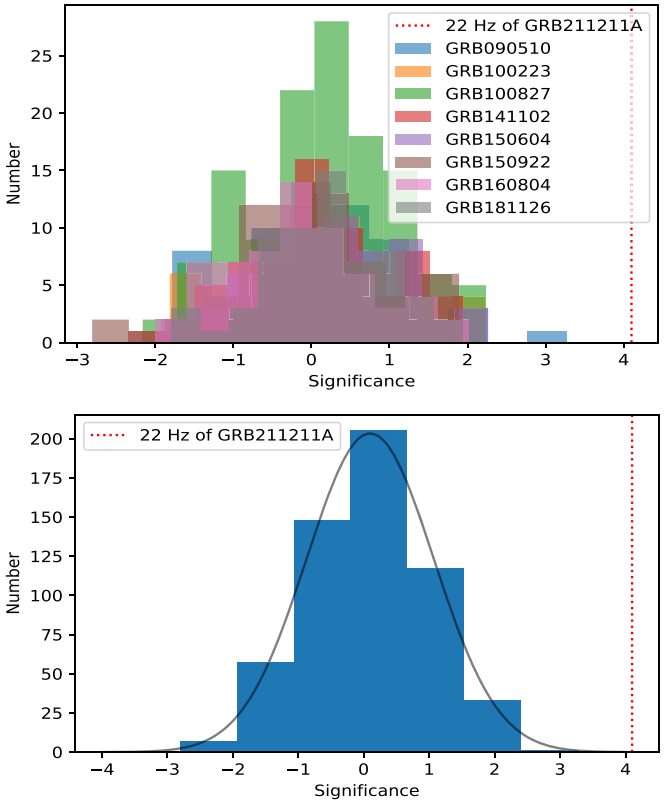

Figure 8. Upper panel: the power significance at different frequencies of the other SGRB precursors with FRED-model subtracted. Lower panel: plot all the histograms in the upper panel into a single histogram; the black line represents the result of fitting a Gaussian function.

uncertainty of the QPO frequency is the full width at half maximum of the peak. We also use another widely used method, the generalized Lomb–Scargle periodogram (Lomb 1976; Scargle 1982; Zechmeister & Kürster 2009) to obtain the power spectra of GBM and BAT lightcurves, which also show strong peaks at $21.93^{+2.82}_{-1.25}$ Hz (GBM) and $21.62^{+2.51}_{-0.63}$ Hz (BAT) (with the period cycle of $45.6^{+2.8}_{-5.2}$ ms (GBM) and $41.5^{+4.8}_{-1.4}$ ms (BAT); Figure 6). The consistency of the two results also shows the reliability of the analysis.

To estimate the confidence level of the above QPO signature found with WWZ, we simulate 2×10^4 artificial lightcurves based on GBM and BAT data using the REDFIT method (Schulz & Mudelsee 2002). The GBM simulation results show that the signal has a 3.0σ confidence level, and the BAT simulation results show that the signal has a 2.0σ confidence level at $\sim$22 Hz. It is worth noting that the REDFIT method needs to satisfy the α of the power-law model for the power spectrum is 2. We find $\alpha = 2.1 \pm 0.1$ (1σ) for the precursor of GRB 211211A.

3.3.5. The Power Spectrum of Other SGRB Precursors with FRED-model Subtracted

To test the validity of using FRED-subtracted precursor lightcurves in the fast Fourier transform, we collect the SGRB precursors (Wang et al. 2020) observed in GBM and use the same procedure to analyze them.

First, we find that the SGRB precursors can be fitted with a single FRED (Xiao et al. 2022b). Then we use the same procedure to obtain their power spectra and then obtain the p-values at different frequencies according to a chi-squared

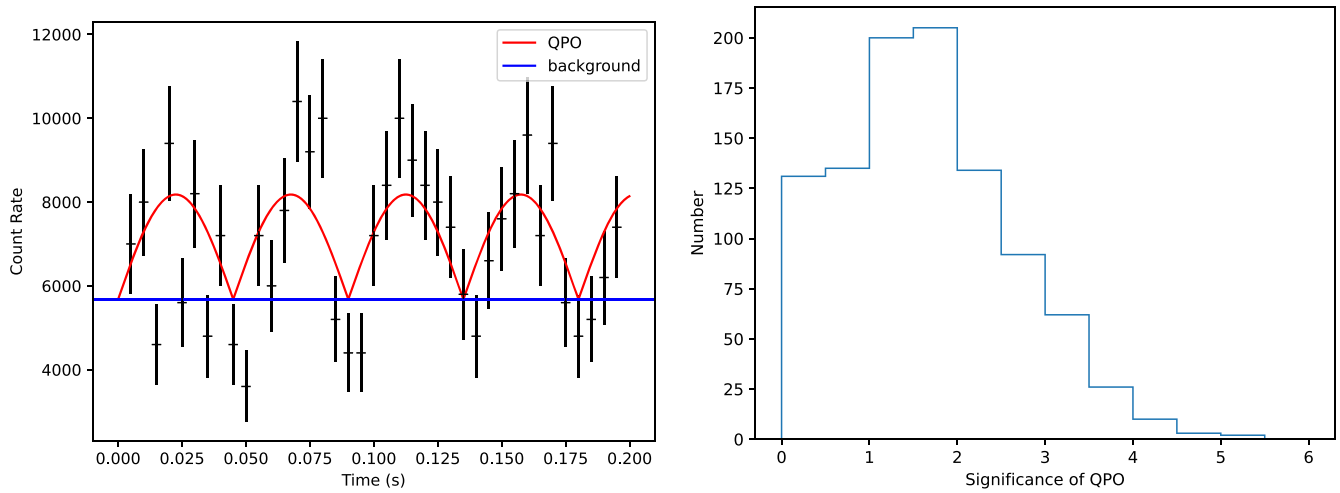

Figure 9. Left panel: a simulated lightcurve of the QPO plus the background based on the duration of the precursor in 211211A and the amplitude and frequency of QPO candidate. Right panel: the distribution of QPO significance calculated from the lightcurves for 1000 simulated observations, there are only two greater than 5σ.

distribution with degrees of freedom (dof) of 2. The corresponding Gaussian significance is obtained and plotted in the histogram (see top panel of Figure 8). We find that they follow a Gaussian distribution well, that is, the SGRB precursors do not have significant red noise after subtracting FRED.

3.3.6. Significance of Simulated Lightcurves

To understand the significance of this QPO, we perform a simulation. As shown in the top right panel in Figure 6, the maximum amplitude of the QPO obtained by the GP is about 20 counts per 8 ms (i.e., 2500 counts per second), and we simulate four half-cycle QPO signals with 22 Hz based on the duration (∼0.2 s) of the precursor, and we use 5700 per second as the background of GBM. It is worth noting here that due to statistical fluctuations, the lightcurves may be different for different observations, thus we simulate 1000 lightcurves and calculate the QPO significance, respectively, using the fast Fourier transform method. The left panel of Figure 9 shows the simulated lightcurve for a single observation, and the right panel is the distribution of significance of QPO, among which there are only two cases greater than 5σ. Besides, the 68% confidence interval for this distribution (corresponding to the 1σ of the Gaussian distribution) is $1.6^{+1.1}_{-0.9}\sigma$, and the QPO significance of the precursor in GRB 211211A observed by GBM is 2.9σ, which is within $\sim 1.2\sigma$ of the distribution. This simulation demonstrates that, even for a real QPO in the observed data, the detection significance of this QPO will not be high in such a short-duration precursor and in such a low-frequency regime as predicted by some magnetar theories (e.g., Sotani et al. 2007; Tews 2017).

We further investigate the significance of QPO with different amplitudes, and repeat the above steps but change the amplitude of QPO. As shown in Figure 10, the value in the horizontal coordinate represents the QPO amplitude, and a value of 1 represents the amplitude of the above simulation based on the precursor of GRB 211211A. The value in vertical coordinate is the QPO significance, and the error bars are 1σ range. Therefore, we can estimate that the QPO observed with significance above 5σ is typically more than twice the amplitude of the precursor of GRB 211211A. Note that for simplicity, the simulation here does not take into account the possible FRED trend or the evolution of the QPO amplitude with time, which may reduce the significance of QPO.

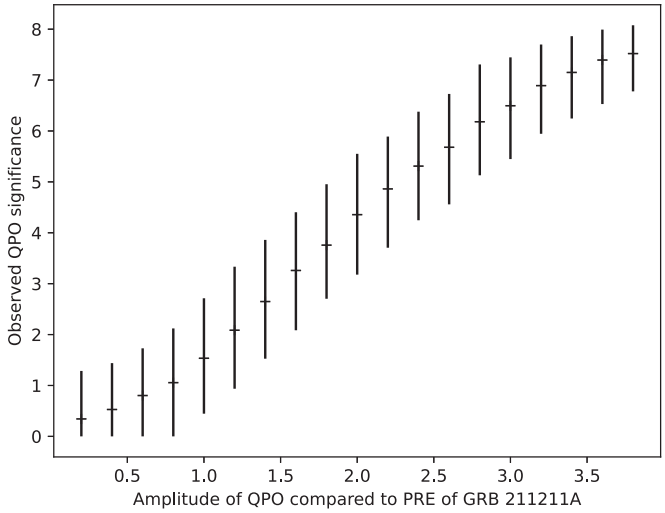

Figure 10. The significance of simulated QPO with different amplitudes. The horizontal coordinate represents the QPO amplitude, 1 represents the amplitude of the simulation based on the precursor of GRB 211211A, and the vertical coordinate is the QPO significance; the error bars are 1σ range.

3.4. Comparison with Other Special Bursts

We compared this precursor of GRB 211211A to the first pulse of other bright GRBs (GRB 130427A, GRB 221009A, and GRB 230307A) to assess whether they share common properties. As shown in Table 4, only GRB 211211A has a precursor that fully satisfies the precursor criteria. For the spectral properties, the precursor of GRB 211211A is softer than the first pulse of GRB 230307A (see Dichiara et al. 2023 for a detailed analysis of the precursor in GRB 230307A.). For the temporal properties, the spectral lag of the precursor of GRB 211211A is similar to the first pulse of GRB 230307A, while the minimum variability timescale of the precursor of GRB 211211A is slightly larger than that of GRB 230307A. This could be the intrinsic difference between them, but we also note that the minimum variability timescale may be dependent on the signal-to-noise ratio (Golkhou et al. 2015).

Table 4
Comparison of the First Episodes of Bright GRBs 211211A, 130427A, 221009A, and 230307A

GRM Name	Energy Spectrum	Spectral Lag (between 8–50 and 100–300 keV) (ms)	Minimum Variability Timescale (8–1000 keV) (ms)	Satisfy the Precursor Criteria
GRB 211211A	CPL, $E_{\rm peak} = 54 \pm 6$ keV, $\alpha = -0.93 \pm 0.28$	10 ± 13	15 ± 2	Yes
GRB 130427A	SBPL, $E_{\rm break} = 291 \pm 23$ keV, $\lambda_1 = -0.334 \pm 0.025$, $\lambda_2 = -3.394 \pm 0.072$ (Ackermann et al. 2014)	224 ± 15	26 ± 15	No (no quiescence period)
GRB 221009A	CPL, $E_{\rm peak} = 3980 \pm 366$ keV, $\alpha = -1.69 \pm 0.01$ (Lesage et al. 2023)	170 ± 87	137 ± 108	No (no quiescence period)
GRB 230307A	Band, $E_{\rm peak} = 170.3 \pm 4.7$ keV, $\alpha = -0.63 \pm 0.04$, $\beta = -2.95 \pm 0.09$ (Dichiara et al. 2023)	12 ± 2	5 ± 1	No (no quiescence period)

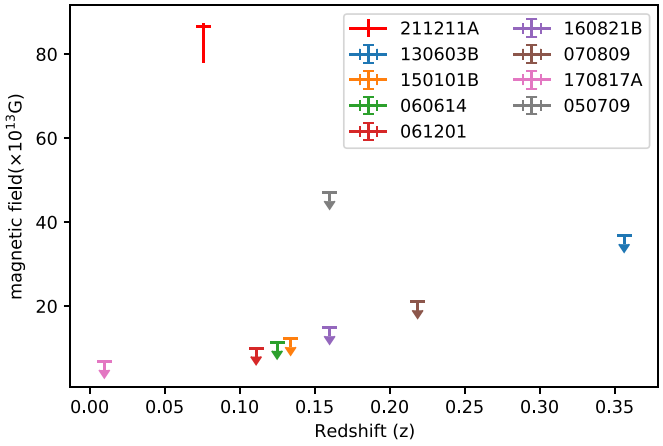

Figure 11. Estimation of neutron star magnetic fields using the premerger magnetosphere interaction model (Hansen & Lyutikov 2001; Abbott et al. 2017) based on the precursors for GRBs with kilonova; the upper limits are calculated based on the sensitivity of the instrument for which no precursors are observed. The magnetic field of GRB 211211A is consistent with the dipole magnetic fields of most known magnetars estimated from their spin-down properties (Olausen & Kaspi 2014).

Besides, a candidate QPO is only found in the precursor of GRB 211211A.

4. Discussion

Considering a binary compact star merger for GRB 211211A, it is difficult to produce strong nonthermal emission in the initial stage of the postmerger phase due to the shielding of ejected material. Indeed, the nonthermal precursors are usually explained by magnetospheric interaction between two neutron stars prior to the merger or the resonant shattering of the crusts of magnetar. Besides, the waiting time between the precursor and main burst ($\sim$1 s) is consistent with the time interval between the binary neutron star merger (ending of the GW signal) and the GRB in GW170817 (Abbott et al. 2017). We therefore suggest that this precursor is most likely produced before the merger.

Interestingly, if invoking the premerger magnetosphere interaction model to explain the luminosity of this precursor, the estimated neutron star magnetic field (using the formula in Hansen & Lyutikov 2001) is $\sim 10^{15}$ G (Figure 11), which is well consistent with a magnetar. In contrast, the upper limits for most other GRBs with kilonova (but without a precursor) are lower than the dipole magnetic fields of most known magnetars (Olausen & Kaspi 2014), making this precursor very special. However, this premerger magnetosphere interaction model seems difficult to give rise to the QPO signal found here.

Despite many efforts to search for QPOs in GRBs, there are only rare bursts reported before the present work (Chirenti et al. 2023). By contrast, QPOs of 10–1000 Hz have been found in several soft gamma-ray repeaters (SGRs), e.g., giant flares of SGR 1806−20 (Watts & Strohmayer 2006) and SGR 1900+14 (Strohmayer & Watts 2005), and an X-ray burst from SGR J1935+2154 and associated with a fast radio burst (FRB200428; Li et al. 2022). They are usually interpreted as the magnetoelastic or crustal oscillations (Samuelsson & Andersson 2007; Gabler et al. 2011; Link & Van Eysden 2016) of a neutron star with an extremely strong magnetic field of $\sim 10^{14-15}$ G (i.e., magnetar). From this point of view, the 22 Hz QPO candidate signal reported here may not be a knotty problem, as long as a magnetar is involved in the progenitor system.

In the magnetar flare scenario, the precursor could be produced by a catastrophic flare accompanied by magnetoelastic or crustal oscillations of the magnetar (Zhang et al. 2022). For this precursor, the flare might be produced $\sim$0.2 s before the coalescence, when the orbital period ($P_{\rm b}$) is $\sim$8 ms and the orbital distance is $\sim$80 km. Since flares and bursts from magnetars are generally considered to be nearly isotropic, or at least not obviously beamed, it is interesting to note that the precursor's total energy output $E_{\rm iso} \sim 7.7 \times 10^{48}$ erg is comparable to the jet-corrected energies E_γ for ME and EE, which are 6.6×10^{48} erg and 2.8×10^{48} erg, respectively. Therefore this precursor of GRB 211211A is energetically very important for this event.

The involvement of magnetar in the merger system may also be supported by the prolonged burst time of GRB 211211A. Numerical relativity simulations show that for the binary merger of highly magnetized neutron stars, the central engine of a GRB would be modeled by a magnetized accretion torus with saturated magnetic field strength (Kiuchi et al. 2014). With the magnetic barrier effect, radial angular momentum transfer may significantly prolong the lifetime of the accretion process (Proga & Zhang 2006; Liu et al. 2012), consistent with the long duration of GRB 211211A.

However, there appears to be a challenge between the relatively short lifetime of a magnetar and the much longer spiraling time ($>$ 86 Myr) of a binary neutron star system due to the GW radiation (Tauris et al. 2017). If the former is much smaller than the latter, it implies that the previous magnetar will no longer be highly magnetized in the late inspiral phase. However, estimating the lifespan of a magnetar and the spiraling time of a binary neutron star system involves many uncertainties. Magnetar age is usually $< \sim 10^4$ yr estimated from their observed period and period derivative as well as the decay of the magnetic field (Kaspi & Beloborodov 2017). If only considering the decay of the magnetic field, it is usually $< \sim 10^7$ yr (Kaspi & Beloborodov 2017; Beniamini et al. 2019). One potentially relevant object is SGR 0418+5729 (Rea et al. 2013), which is apparently much older ($\sim 3.6 \times 10^7$ yr; Beniamini et al. 2019), but it may still not be old enough to explain GRB 211211A. However, there is no consensus on the timescale of magnetic field decay. Additionally, the spiraling time is heavily influenced by the initial orbit of the inspiral during its formation and the environment surrounding the binary system. Another possibility is that the weak magnetic field of a neutron star can be amplified up to a strength of $\sim 10^{15}$ G during the late spiraling phase, which means that an old neutron star may be recycled into a magnetar in this process (Dall'Osso & Rossi 2013).

In addition, as the binary period decreases, crust oscillations could become stronger and stronger. From the top right panel in Figure 6, the QPO amplitude seems to first increase slightly and then decrease slowly (similar to the QPO in another magnetar burst; Li et al. 2022); this is not fully consistent with the aforementioned expectation if the observed QPO amplitude is positively correlated with the strength of the crust oscillations. On the other hand, it is unclear how the QPO amplitude in X-ray/Gamma-ray flux is related to the strength of the crust oscillations, which also requires more theoretical calculations.

5. Summary

In this work, we report a peculiar precursor in the GRB 211211A, whose temporal and spectral characteristics are

different from that of the main emission and extended emission of GRB 211211A. We find that this precursor is a rare case with a high-confident nonthermal spectrum in a GRB originating from a binary merger.

In particular, we find that there is a QPO candidate in the precursor. We utilize a series of temporal and frequency domain QPO search methods, including GP, Z^2, fast Fourier transform, and WWZ methods, to calculate the significance, and obtain 2.5σ, 6.6σ, 2.9σ, and 3.0σ observed by GBM, respectively. Considering all these results, we summarize that the significance of the QPO candidate should be $\sim 3\sigma$. We note that the QPO significance ($\sim 7\sigma$) found in GRB 200415A using the Z^2 method (Castro-Tirado et al. 2021) is close to that (6.6σ) of this precursor in GRB 211211A. In addition, we searched for a QPO in the precursors of the other SGRBs using the same methods but did not find any significant signal; that is, the significance of the QPO candidate in the precursor of GRB 211211A is the highest among all precursors of SGRBs. Moreover, our simulations illustrate that it is difficult to obtain highly significant low-frequency QPO in such a short precursor, lending additional support to the QPO signal found in GRB 211211A.

We suggest that this peculiar precursor could be explained either by the premerger magnetosphere interaction model or the magnetar crustal oscillations model. For the former, the magnetic field of the neutron star is estimated to be $\sim 10^{15}$ G, which is well consistent with a magnetar. For the latter, a magnetar catastrophic flare (or called superflare) can also well explain the characteristics of the precursor, especially the QPO feature (Zhang et al. 2022). Thus, we conclude that both models point toward the magnetar involvement in the merger. Interestingly, the strong magnetic field of the magnetar can naturally lead to the prolonged duration of GRB 211211A, which is otherwise difficult to explain. Meanwhile, more theoretical discussions have been proposed to interpret the observation features of this peculiar precursor (Suvorov et al. 2022; Zhang et al. 2022; Sullivan et al. 2024).

Finally, gravitational waveforms of magnetized and nonmagnetized neutron star binaries could be well distinguished as long as the neutron star magnetic field is strong enough (Giacomazzo et al. 2009). Future multimessenger observations have the potential to confirm the presence of highly magnetized neutron stars as progenitors of bursts similar to GRB 211211A and to determine if their precursors are produced by magnetar flares. Furthermore, these observations could provide valuable insights into the physical mechanism underlying the precursors and their intriguing behaviors, including possible QPOs.

Acknowledgments

This work made use of the data from the Insight-HXMT, Fermi, and Swift. This work is supported by the National Key R&D Program of China (2021YFA0718500), the National Natural Science Foundation of China (Nos. 12303043 and 12273042, Projects: 12061131007 and 12021003), the Strategic Priority Research Program (grant Nos. XDA30050000, XDB0550300, XDA15052700, and XDB23040400) of the Chinese Academy of Sciences, and the International Partnership Program of Chinese Academy of Sciences (grant No. 113111KYSB20190020). D.X. acknowledges the support by the Strategic Priority Research Program "Multi-wavelength Gravitational Wave Universe" of the CAS (No. XDB23000000) and the science research grants from the China Manned Space Project with Nos. CMS-CSST-2021-A13 and CMS-CSST-2021-B11. We thank Xing Gao for the kind help of the Nanshan/NEXT observations. We thank Bing Zhang and Daniela Huppenkothen for the helpful discussions. We acknowledge the support of the staff of the Xinglong 2.16 m telescope. This work was also partially supported by the Open Project Program of the Key Laboratory of Optical Astronomy, National Astronomical Observatories, Chinese Academy of Sciences.

ORCID iDs

Shuo Xiao https://orcid.org/0000-0003-2957-2806
Zi-Pei Zhu https://orcid.org/0000-0002-9022-1928
Shao-Lin Xiong https://orcid.org/0000-0002-4771-7653
He Gao https://orcid.org/0000-0002-3100-6558
Dong Xu https://orcid.org/0000-0003-3257-9435
Shuang-Nan Zhang https://orcid.org/0000-0001-5586-1017
Xiao-Bo Li https://orcid.org/0000-0003-4585-589X
Fang-Jun Lu https://orcid.org/0000-0003-3248-6087
Lin Lin https://orcid.org/0000-0002-0633-5325
Liang-Duan Liu https://orcid.org/0000-0002-8708-0597
Zhen Zhang https://orcid.org/0000-0003-4673-773X
Ming-Yu Ge https://orcid.org/0000-0002-2749-6638
You-Li Tuo https://orcid.org/0000-0003-3127-0110
Tian-Cong Wang https://orcid.org/0000-0002-9332-5562
Zhou-Jian Cao https://orcid.org/0000-0002-1932-7295
Shu-Xu Yi https://orcid.org/0000-0001-7599-0174
Xi-Lu Wang https://orcid.org/0000-0002-5901-9879
Ce Cai https://orcid.org/0000-0002-6540-2372
Sheng-Lun Xie https://orcid.org/0000-0001-9217-7070
Cheng-Kui Li https://orcid.org/0000-0001-5798-4491
Li-Ming Song https://orcid.org/0000-0003-0274-3396
Jin-Lu Qu https://orcid.org/0000-0002-9796-2585
Xu-Fang Li https://orcid.org/0000-0002-2793-9857
Yu-Peng Xu https://orcid.org/0000-0002-8476-9217

References

Abbott, B. P., Abbott, R., Abbott, T., et al. 2017, ApJL, 848, L13
Ackermann, M., Ajello, M., Asano, K., et al. 2014, Sci, 343, 42
Amati, L., Frontera, F., Tavani, M., et al. 2002, A&A, 390, 81
Bachetti, M., Huppenkothen, D., Khan, U., et al. 2022, StingraySoftware/stingray, v1.0, Zenodo, doi:10.5281/zenodo.6394742
Beniamini, P., Hotokezaka, K., Van Der Horst, A., & Kouveliotou, C. 2019, MNRAS, 487, 1426
Bloom, J. S., Kulkarni, S. R., & Djorgovski, S. G. 2002, AJ, 123, 1111
Castro-Tirado, A. J., Østgaard, N., Gögüş, E., et al. 2021, Natur, 600, 621
Chirenti, C., Dichiara, S., Lien, A., Miller, M. C., & Preece, R. 2023, Natur, 613, 253
D'Ai, A., Ambrosi, E., D'Elia, V., et al. 2021, GCN, 31202, 1
Dall'Osso, S., & Rossi, E. M. 2013, MNRAS, 428, 518
Dichiara, S., Tsang, D., Troja, E., et al. 2023, ApJL, 954, L29
Foster, G. 1996, AJ, 112, 1709
Gabler, M., Cerdá-Durán, P., Font, J. A., Müller, E., & Stergioulas, N. 2011, JPhCS, 283, 012013
Giacomazzo, B., Rezzolla, L., & Baiotti, L. 2009, MNRAS: Lett., 399, L164
Gillanders, J. H., Troja, E., Fryer, C. L., et al. 2023, arXiv:2308.00633
Golkhou, V. Z., Butler, N. R., & Littlejohns, O. M. 2015, ApJ, 811, 93
Gompertz, B. P., Ravasio, M. E., Nicholl, M., et al. 2023, NatAs, 7, 67
Hansen, B. M., & Lyutikov, M. 2001, MNRAS, 322, 695
Hu, Y.-D., Liang, E.-W., Xi, S.-Q., et al. 2014, ApJ, 789, 145
Hübner, M., Huppenkothen, D., Lasky, P. D., & Inglis, A. R. 2022a, ApJS, 259, 32
Hübner, M., Huppenkothen, D., Lasky, P. D., et al. 2022b, ApJ, 936, 17
Jin, Z.-P., Covino, S., Liao, N.-H., et al. 2020, NatAs, 4, 77
Kaspi, V. M., & Beloborodov, A. M. 2017, ARA&A, 55, 261
Kiuchi, K., Kyutoku, K., Sekiguchi, Y., Shibata, M., & Wada, T. 2014, PhRvD, 90, 041502
Kouveliotou, C., Meegan, C. A., Fishman, G. J., et al. 1993, ApJ, 413, L101
Lesage, S., Veres, P., Briggs, M., et al. 2023, ApJL, 952, L42
Levan, A., Gompertz, B. P., Salafia, O. S., et al. 2024, Natur, 626, 737

Li, L., & Mao, J. 2022, ApJ, 928, 152
Li, L.-X., & Paczyński, B. 1998, ApJ, 507, L59
Li, T.-P., & Ma, Y.-Q. 1983, ApJ, 272, 317
Li, T.-P., Qu, J.-L., Feng, H., et al. 2004, ChJAA, 4, 583
Li, X., Ge, M., Lin, L., et al. 2022, ApJ, 931, 56
Liddle, A. R. 2007, MNRAS: Lett., 377, L74
Link, B., & Van Eysden, C. A. 2016, ApJL, 823, L1
Liu, T., Liang, E.-W., Gu, W.-M., et al. 2012, ApJ, 760, 63
Lomb, N. R. 1976, Ap&SS, 39, 447
Malesani, D., Fynbo, J., de Ugarte Postigo, A., et al. 2021, GCN, 31221, 1
Mangan, J., Dunwoody, R., Meegan, C. & Fermi GBM Team 2021, GCN, 31210, 1
Mei, A., Banerjee, B., Oganesyan, G., et al. 2022, Natur, 612, 236
O'Connor, B., Troja, E., Dichiara, S., et al. 2021, MNRAS, 502, 1279
Olausen, S., & Kaspi, V. 2014, ApJS, 212, 6
Palenzuela, C., Lehner, L., Ponce, M., et al. 2013, PhRvL, 111, 061105
Proga, D., & Zhang, B. 2006, MNRAS: Lett., 370, L61
Rastinejad, J. C., Gompertz, B. P., Levan, A. J., et al. 2022, Natur, 612, 223
Rea, N., Israel, G. L., Pons, J. A., et al. 2013, ApJ, 770, 65
Samuelsson, L., & Andersson, N. 2007, MNRAS, 374, 256
Scargle, J. D. 1982, ApJ, 263, 835
Scargle, J. D., Norris, J. P., Jackson, B., & Chiang, J. 2013, ApJ, 764, 167
Schulz, M., & Mudelsee, M. 2002, CG, 28, 421
Schwarz, G. 1978, AnSta, 6, 461
Sotani, H., Kokkotas, K., & Stergioulas, N. 2007, MNRAS, 375, 261
Strohmayer, T. E., & Watts, A. L. 2005, ApJ, 632, L111
Sullivan, A. G., Alves, L. M., Márka, Z., Bartos, I., & Márka, S. 2024, MNRAS, 527, 7722
Suvorov, A. G., Kuan, H.-J., & Kokkotas, K. D. 2022, A&A, 664, A177
Tauris, T., Kramer, M., Freire, P., et al. 2017, ApJ, 846, 170
Tews, I. 2017, PhRvC, 95, 015803
Troja, E., Fryer, C., O'Connor, B., et al. 2022, Natur, 612, 228
Troja, E., Rosswog, S., & Gehrels, N. 2010, ApJ, 723, 1711
Tsang, D., Read, J. S., Hinderer, T., Piro, A. L., & Bondarescu, R. 2012, PhRvL, 108, 011102
Van der Klis, M. 1989, in Timing Neutron Stars (Berlin: Springer), 27
Wang, J.-S., Peng, F.-K., Wu, K., & Dai, Z.-G. 2018, ApJ, 868, 19
Wang, J.-S., Peng, Z.-K., Zou, J.-H., Zhang, B.-B., & Zhang, B. 2020, ApJL, 902, L42
Watts, A. L., & Strohmayer, T. E. 2006, ApJ, 637, L117
Woosley, S., & Bloom, J. 2006, ARA&A, 44, 507
Wu, M.-R., Tamborra, I., Just, O., & Janka, H.-T. 2017, PhRvD, 96, 123015
Xiao, S., Peng, W.-X., Zhang, S.-N., et al. 2022b, ApJ, 941, 166
Xiao, S., Xiong, S.-L., Wang, Y., et al. 2022a, ApJL, 924, L29
Xiao, S., Yang, J.-J., Luo, X.-H., et al. 2023, ApJS, 268, 5
Yang, J., Ai, S., Zhang, B.-B., et al. 2022, Natur, 612, 232
Yang, Y.-H., Troja, E., O'Connor, B., et al. 2024, Natur, 626, 742
Zechmeister, M., & Kürster, M. 2009, A&A, 496, 577
Zhang, B. 2018, The Physics of Gamma-ray Bursts (Cambridge: Cambridge Univ. Press)
Zhang, B., Zhang, B.-B., Virgili, F. J., et al. 2009, ApJ, 703, 1696
Zhang, Y., Xiong, S., Li, X., et al. 2021, GCN, 31236, 1
Zhang, Z., Yi, S.-X., Zhang, S.-N., Xiong, S.-L., & Xiao, S. 2022, ApJL, 939, L25
Zhong, S.-Q., Dai, Z.-G., Cheng, J.-G., Lan, L., & Zhang, H.-M. 2019, ApJ, 884, 25